Chapter 4

Solid-state microwave modification of precipitated Fischer-Tropsch catalysts: The effect of potassium

4.1 Introduction

Fischer-Tropsch synthesis (FTS) is a well-established catalytic process used to convert syngas (H_2 and CO) derived from coal or natural gas to transportation fuels and petrochemical substitutes.[1-4] Upon combustion FTS derived diesel fuel, compared with conventional diesel fuel, not only gives low nitrogen oxides (NO_x), carbon monoxide (CO) and hydrocarbon (HC) emissions, but also much lower nano-particulate matter emissions which are suspected of being a leading health threat.[5]

Iron-based catalysts are often used in commercial operations, especially for coal derived syngas with a low H_2/CO ratio. This in part is due to their high water gas shift (WGS) activity, low cost, flexible operating conditions as well as the reasonable product distribution produced.[6-8] To improve the FTS performance (activity, selectivity and stability) of iron-based catalysts, much effort has been expended on studying the effect of the addition of electronic or structural promoters to the catalyst.[9] Potassium is normally used as an electronic promoter for iron-based catalysts. Yang *et al.*[10] studied precipitated catalysts with the potassium loading varying between 0 and 3.0 wt. % K, and they reported 0.7 wt. % K as the optimum potassium loading; FTS and water-gas shift (WGS) activity were the highest observed for this catalyst.

Recent studies have emphasized the importance and development of a robust, active catalyst suitable for the production of transportation fuels (high-alpha value catalyst).[11] To further generate novel catalysts with even better performance, new methods to prepare catalysts are required. One method that has been little studied is the use of microwave heating. Linganiso[12] has shown that microwave pre-treatment improved the performance of iron-based FTS

catalysts. This study suggested that the procedure led to interesting results. Further explanation of this approach provides the basis for this chapter. Herein, a study aimed at establishing the presence of microwave induced effects on precipitated catalysts was undertaken. The effect of potassium loading and the irradiation time dependency of the microwave effect was investigated.

4.2 Experimental

Unsupported catalysts were prepared by the continuous precipitation technique as explained in Chapter 3. For brevity, the unpromoted sample is referred to as 0K/Fe and the potassium promoted ones are denoted as *x*K/Fe, where *x* is the weight percent of potassium in the samples. The value of *x* varied between 0.2 and 1.5. This labelling format was used for the non-microwaved samples. After successful preparation, the samples were then irradiated with microwaves in an attempt to modify their bulk and surface properties. The samples were microwaved at a power level of 450 W for 10 seconds. The effect of the microwave pre-treatment time has also been studied. For the microwaved samples, the unpromoted sample is denoted as 0K/Fe-MW and the potassium promoted ones are represented as *x*K/Fe-MW. Techniques used in this study include TEM, BET, XRD, TPR and TPSR-MS. Further details on how the experiments were performed are discussed in Chapter 3.

4.3 Results and discussion

4.3.1 Transmission electron microscopy (TEM)

Particle size analysis of the unsupported catalysts was done after calcination of the samples at 350 ^{o}C for 6.5 hours. Six non-microwaved samples were analysed using TEM, namely 0K/Fe, 0.2K/Fe, 0.5K/Fe, 0.7K/Fe, 1.0K/Fe and 1.5K/Fe. Figure 4.1a and 4.1b compares the TEM images of 0.5K/Fe and 0.7K/Fe catalysts, in that order. TEM results for the other non-microwaved samples are shown in Appendix A. For each sample a total of 300 particles were counted and analysed, the percentage size distributions obtained were plotted in Figure 4.1c and 4.1d. The sample loaded with 0.5 weight percent potassium had an average particle size of 21 nm while the 0.7K/Fe sample had an average particle size of 22 nm. The particles

prepared in the two catalysts are near spherical in shape as can be seen from the TEM images. The effect of potassium on the particle size of the various non-microwaved catalysts is summarized in Table 4.1.

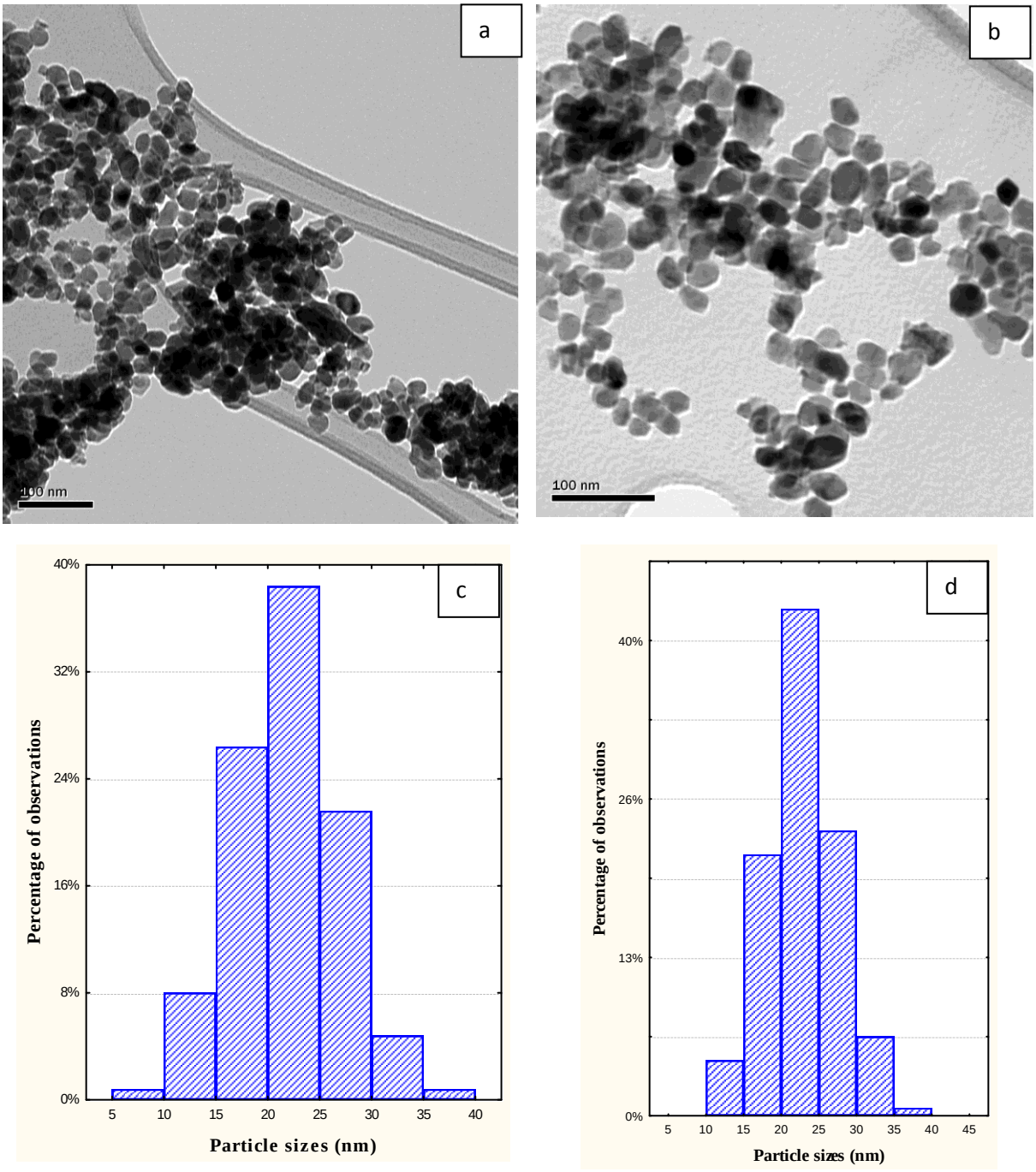

Figure 4.1 TEM images of (a) 0.5 K/Fe and (b) 0.7 K/Fe catalysts. The corresponding particle size distributions are shown in (c) and (d).

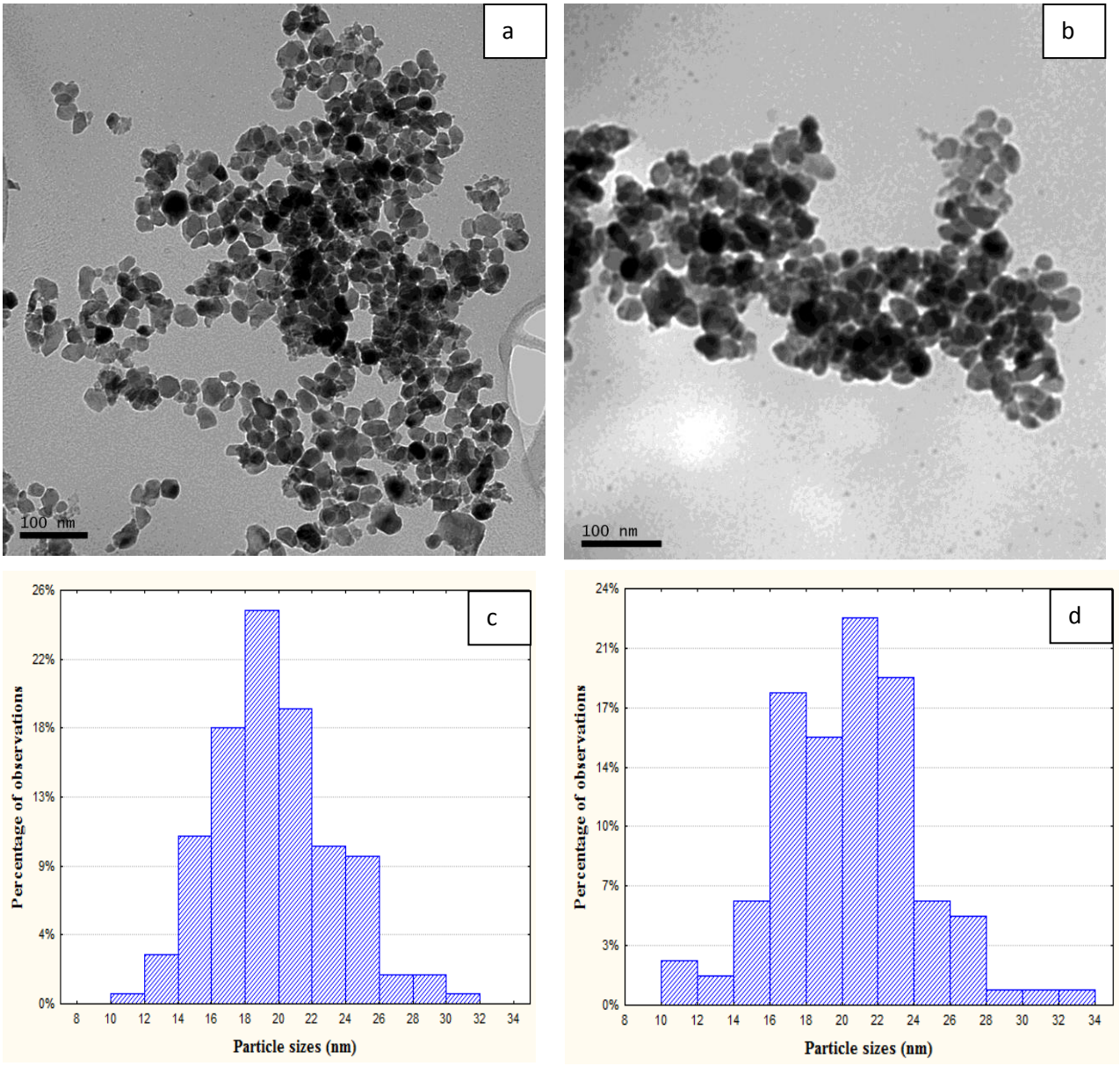

Figure 4.2 TEM images of (a) 0K/Fe-MW and (b) 0.5K/Fe-MW catalysts. These samples were microwaved for 10 seconds (450 W). The corresponding particle size distributions are shown in (c) and (d).

Figure 4.2 shows images from the 0K/Fe-MW and 0.5K/Fe-MW samples and the corresponding particle size distributions. The effect of potassium on the particle size of the microwaved catalysts is illustrated in Table 4.1. From Table 4.1 it can be seen that the average particle size varies between 18 and 28 nm for all the samples. The iron particles were observed to increase slightly with an increase in the content of potassium in the catalysts. This trend is present in both the microwaved and non-microwaved samples. Microwave pre-treatment was seen not to affect the sample's average particle size as data obtained from the

microwaved samples was almost similar to the values obtained from their non-microwaved counterparts.

X-ray diffraction (XRD) and Mossbauer emission spectroscopy (MES) have also been used in the literature[10] to draw a similar conclusion on the effect of potassium promoter on precipitated iron catalysts: that samples containing potassium have larger crystallites than samples without potassium.

Table 4.1 Average iron particle sizes in the catalysts with different loadings of potassium. Microwave pre-treatment conditions: 450 W power level, 10 seconds.

Catalyst	**Average particle size (nm)**	
	Non-microwaved samples	Microwaved samples
0K/Fe	19	18
0.2K/Fe	19	20
0.5K/Fe	21	21
0.7K/Fe	22	21
1.0K/Fe	22	23
1.5K/Fe	26	28

4.3.2 Porosity studies

The surface areas and pore volumes of the various catalysts were calculated from N_2 adsorption-desorption isotherms. To determine if there was any structure modification to the catalysts during microwave pre-treatment, N_2 adsorption-desorption isotherms of the various microwaved and non-microwaved catalysts were compared [see Figure 4.3, 4.4 and 4.5]. In these figures adsorption curves are shown in black whereas desorption curves are shown in

red. The N_2 adsorption-desorption isotherm associated with the catalysts studied here can be accounted for as a Type V isotherm, according to the IUPAC classification.[13,14] Here the volume of the gas adsorbed increases without limit as its relative saturation approaches unity. The sharp condensation step in the adsorption and desorption curves of Type IV isotherm is absent in these isotherms. The adsorption and desorption branches of the isotherms are not coincident, exhibiting a hysteresis loop between $P/P_o = 0.5$ and $P/P_o = 0.9$ for all the catalysts. This is due to capillary condensation augmenting multilayer adsorption at these relative pressures at which hysteresis is present. The occurrence of hysteresis loops is also evidence for mesoporosity in these catalysts.[15] Mesoporous materials are materials that have pore diameters between 2 and 50 nm.

Considering the adsorption behaviour of all the isotherms before and after microwave pre-treatment for the various loadings of potassium, it can be seen that their shapes all look similar. This clearly shows that microwave pre-treatment does not significantly modify the accessible structure of the catalyst.

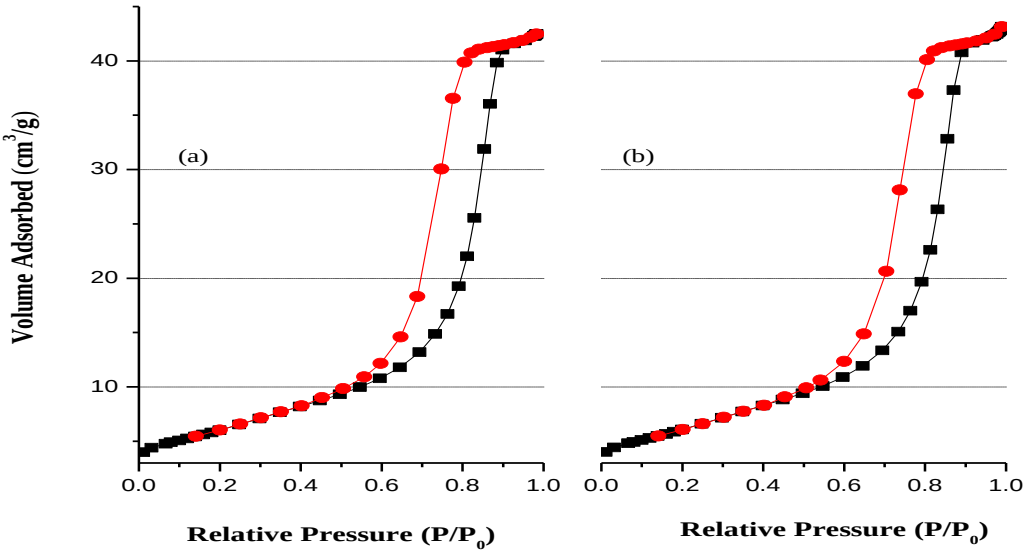

Figure 4.3 Adsorption-desorption isotherms for unsupported 0K/Fe (a) without microwave pre-treatment and (b) after microwave pre-treatment. Microwave pre-treatment conditions: 450 W power level, 10 seconds. Adsorption curves are shown in black whereas desorption curves are shown in red.

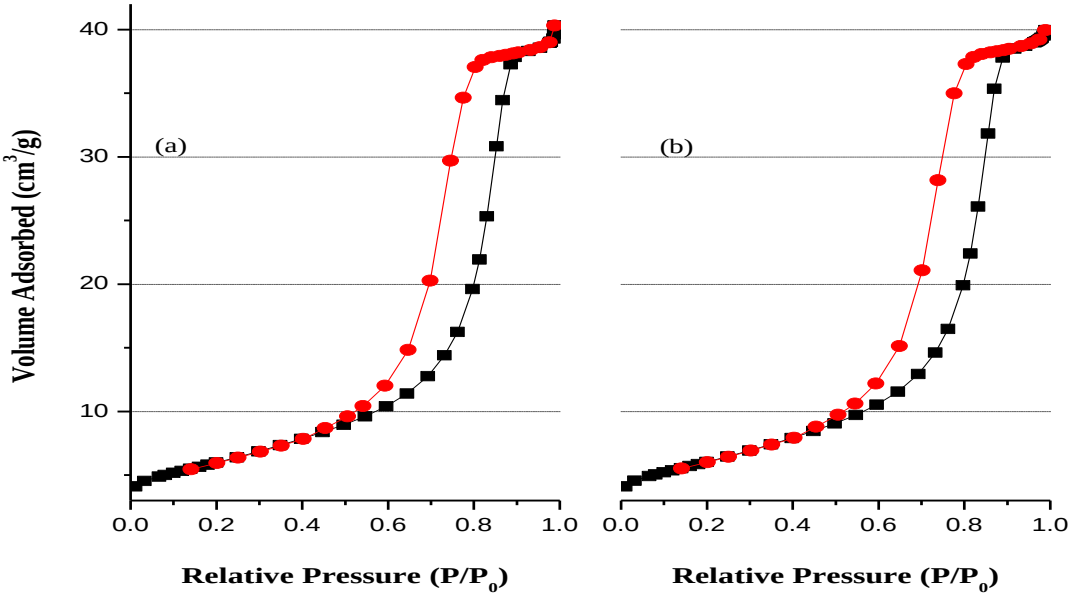

Figure 4.4 Adsorption-desorption isotherms for unsupported 0.7K/Fe catalysts (a) without microwave pre-treatment and (b) after microwave pre-treatment. Adsorption curves are shown in black whereas desorption curves are shown in red.

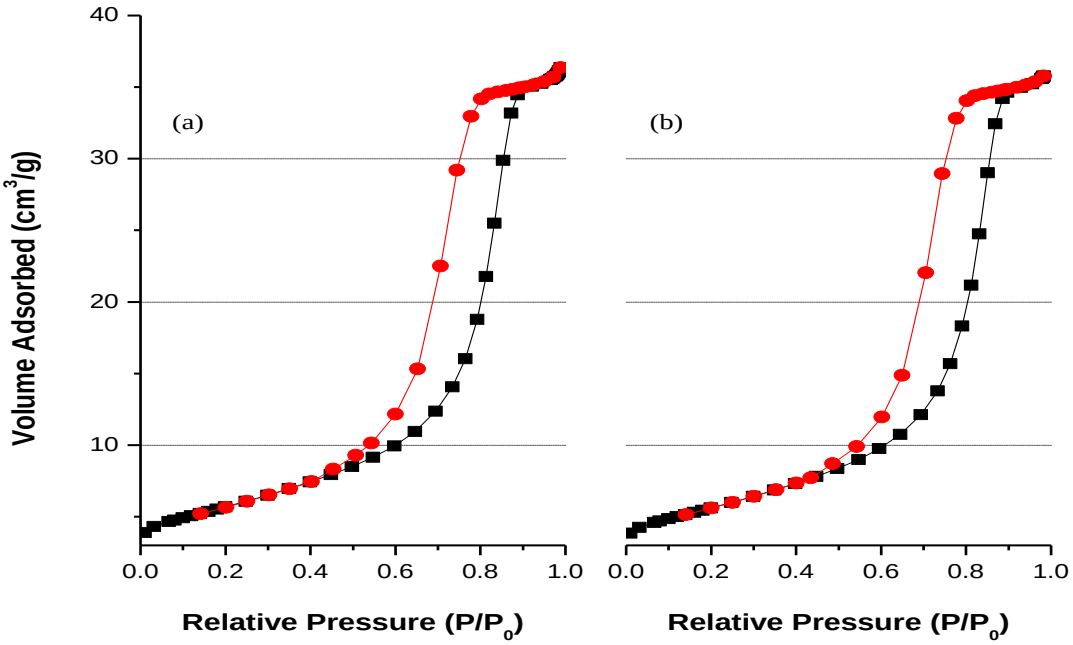

Figure 4.5 Adsorption-desorption isotherms for unsupported 1.5K/Fe catalysts (a) without microwave and (b) after microwave pre-treatment. Adsorption curves are shown in black whereas desorption curves are shown in red. Microwave pre-treatment conditions: 450 W power level, 10 seconds.

Surface area and pore volume measurements were determined before and after microwave pre-treatment using the Brunauett-Emmett-Teller (BET) method and the results are tabulated in Table 4.2. The BET surface areas of all the catalysts are in the range of 19 – 22 m^2/g, while pore volumes fall in the range 0.05 – 0.07 cm^3/g. It is apparent that the surface area does not change significantly with the addition of more potassium, except for the 1.5 K/Fe catalyst which shows a small decrease in surface area. This decrease in surface area is due to the fact that potassium improves the agglomeration of the FeOOH precursor and further enlarges the crystallite size of α-Fe_2O_3 after calcination.[10] Particle size analysis from TEM also confirmed this. The pore volume was found to decrease consistently with increasing potassium. However, microwave pre-treatment of the catalysts was found to have no effect on the surface area and the pore volume of the different catalysts.

Table 4.2 Textural properties of the catalyst as prepared before and after microwave pre-treatment.

Catalyst composition (parts by wt.)	**BET surface area* (m^2/g)**		**Pore volume* (cm^3/g)**	
	A	B	A	B
100Fe	20.2	20.3	0.066	0.066
0.2K/Fe	20.7	20.7	0.064	0.064
0.5K/Fe	20.4	20.6	0.062	0.063
0.7K/Fe	20.6	20.7	0.060	0.061
1.0K/Fe	21.2	21.1	0.059	0.059
1.5K/Fe	19.2	19.6	0.055	0.056

*Maximum error = ± 2%

A = Without any microwave pre-treatment; B = Values obtained after 10 seconds of microwave pre-treatment (450 W)

The corresponding pore size distribution for the various unsupported catalysts were calculated from the desorption branches of the nitrogen isotherm by the Barrett-Joyner-Halenda (BJH) method.[16] The analysis revealed that the pore size distribution is narrow (see

Figure 4.6). These pore sizes are within the range of those that correspond to mesopores (2 to 50 nm).[15] The average pore diameter was found to be unchanged (12.8 and 12.4 nm) for loadings of potassium between 0.2 and 1.5 weight percent. Type V isotherms are normally associated with agglomerates or compacts of uniform spheres in a fairly regular array and hence gives a narrow distribution of pore sizes. A very small (marginal) decrease in the pore volume is also observed as the loading of potassium is increased, which suggests that potassium occupies pores in the catalyst thus blocking them. Microwave pre-treatment was found not to alter the pore size distribution since similar results were obtained for the MW modified catalysts.

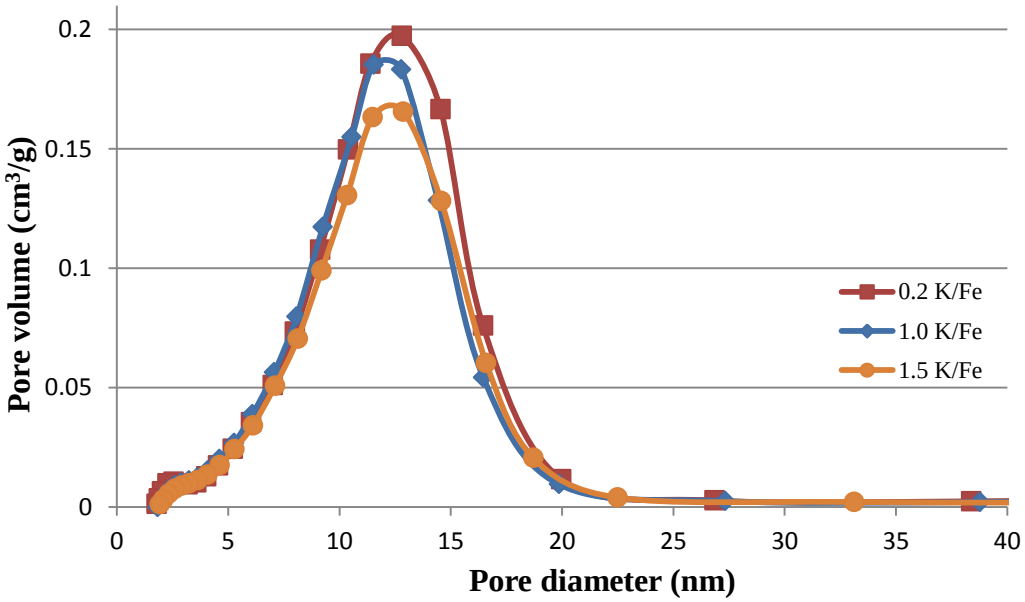

Figure 4.6 Pore size distributions of precipitated K/Fe catalysts, with potassium loadings of 0.2, 1.0 and 1.5 weight percentage. These pore size distributions were obtained from non-microwaved samples.

4.3.3 X-ray Diffraction (XRD)

Powder X-ray diffraction patterns for the various precipitated catalysts with potassium contents ranging between 0 to 1.5 weight percent are shown in Figure 4.7. The XRD patterns were plotted over 2θ values ranging from 10 to 90°. The main detectable crystallographic phase present in all the diffraction patterns is hematite (α-Fe_2O_3), which has characteristic

peaks at 2θ values of 24.2, 33.1, 35.6, 40.8, 49.52, 54.0, 57.6, 62.5 and 64.0°.[10] All the patterns look the same except for the peak at a 2θ value of 30° which increases with the loading of potassium. This signal is due to potassium in the form of K_2O. Microwave pre-treatment did not affect the phases present as the patterns obtained after pre-treatment were similar to those recorded for non-microwaved samples.

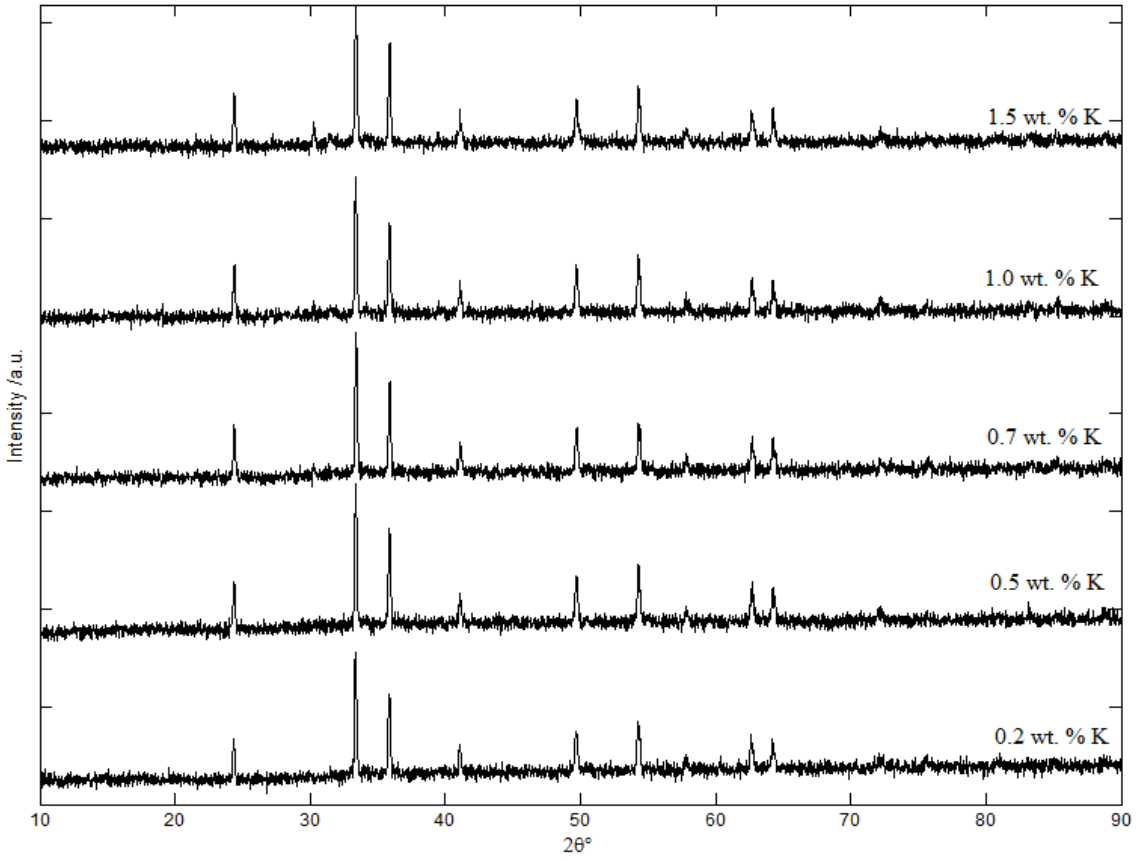

Figure 4.7 X-ray diffraction patterns for the various precipitated catalysts before microwave pre-treatment.

Estimation of the Fe_2O_3 crystallite sizes in the various samples was done *via* the Scherrer equation and the data obtained is listed in Table 4.3. The crystallite sizes ranged between 27.9 and 36.1 nm for both microwaved and non-microwaved samples. For the non-microwaved samples, it was observed that the crystallite sizes increased as the content of the potassium promoter was increased in the catalysts. This behaviour was also duplicated in the

microwaved samples and suggests that pre-treatment does not affect the particle size of these catalysts.

Table 4.3 Fe_2O_3 crystallite sizes as determined using the Scherrer equation. Microwave pre-treatment conditions: 450 W power level, 10 seconds.

Catalyst	**Crystallite size (nm)**[a]	
	Non-microwaved samples	Microwaved samples
0.2K/Fe	28.9	27.9
0.5K/Fe	32.1	32.1
0.7K/Fe	34.7	34.7
1.0K/Fe	34.7	36.1
1.5K/Fe	36.1	36.1

[a]Maximum error = ± 5%

4.3.4 Temperature programmed reduction (TPR)

4.3.4.1 Non-microwave pre-treated samples

The effect of potassium on the reduction behaviour of unsupported catalysts was studied using temperature programmed reduction (TPR) with H_2 as the reductant gas. Figure 4.8 shows the TPR profiles of 0.2K/Fe, 0.5K/Fe, 0.7K/Fe and 1.5K/Fe catalysts that were not pre-treated using microwave radiation. All these catalysts were found to undergo a two-step reduction that is ascribed to the reduction of Fe_2O_3 to Fe_3O_4 (peak 1, equation 4.1) and Fe_3O_4 to Fe^0 (peak 2, equation 4.2).[17]

$$3\ Fe_2O_3 + H_2 \rightarrow 2\ Fe_3O_4 + H_2O \qquad 4.1$$

$$Fe_3O_4 + 4\ H_2 \rightarrow 3\ Fe^0 + 4\ H_2O \qquad 4.2$$

The exact positions for Peak 1 and Peak 2 for the different catalysts are listed in Table 4.4. The first reduction peak shifts significantly to higher temperatures as the loading of potassium is increased, indicating that the reduction of the catalyst is inhibited by the addition of potassium. This may be the result of the strong interaction between potassium oxide and iron oxide. The strong interaction of potassium oxide with iron oxide could suppress the adsorption of hydrogen on the catalyst surface and therefore restrain the reduction of iron oxide underlying and/or neighbouring the potassium promoter.[18,19] The increase in particle size of the crystallites seen in TEM could also lead to a decrease in the surface area exposed to the H_2 reductant; this could also lead to the reduction behaviour displayed in Figure 4.8. Studies done by Li using temperature programmed and isothermal reduction at 573 K also showed that potassium retarded the reduction of iron when H_2 was used as the reductant.[20] Unlike Peak 1, the shift to high temperatures for Peak 2 is not as pronounced in the various samples.

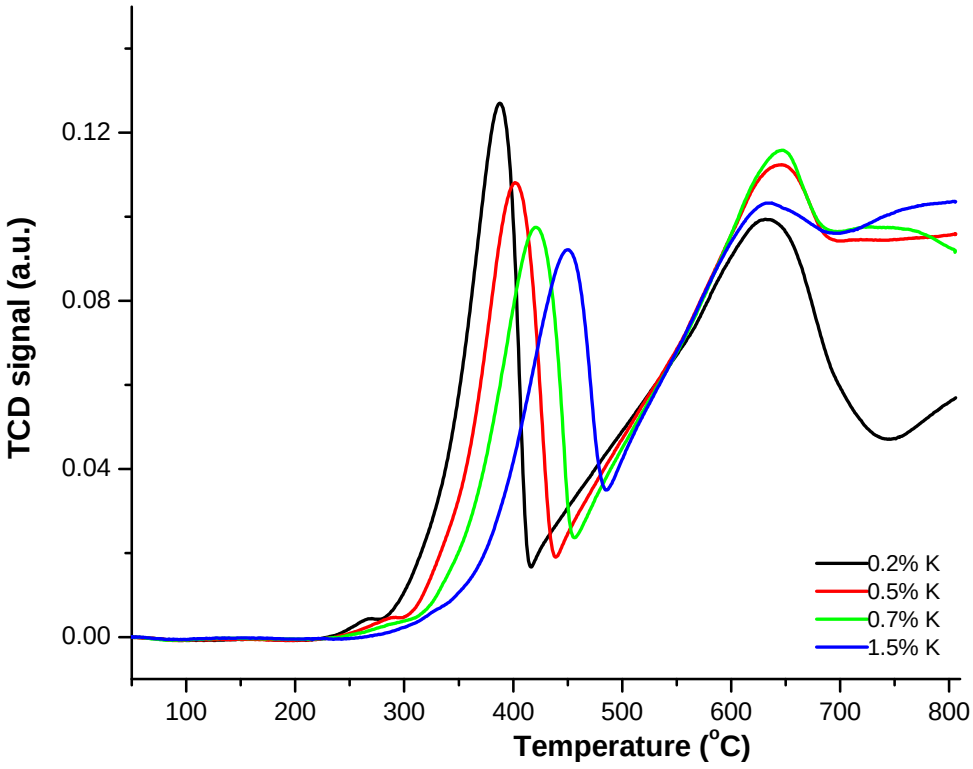

Figure 4.8 Reduction profiles of K/Fe-type catalysts prior to microwave pre-treatment, with potassium loadings of 0.2, 0.5, 0.7 and 1.5 wt. %. TPR conditions: 5% H_2/N_2, 25 – 800 ^oC, 10 ^oC/min.

Table 4.4 Reduction temperatures for the H_2-TPR profiles shown in Figure 4.8 and Figure 4.9. Microwave pre-treatment conditions: 450 W power level, 10 seconds.

Sample	Non-microwaved samples (^oC)		Microwaved samples (^oC)	
	Peak 1	**Peak 2**	**Peak 1**	**Peak 2**
0K/Fe	380	594	376	589
0.2 K/Fe	387	632	385	631
0.5 K/Fe	402	636	407	657
0.7 K/Fe	421	646	420	661
1.0 K/Fe	431	646	431	647
1.5 K/Fe	450	646	448	643

4.3.4.2 Microwave pre-treated samples

Fresh catalysts were exposed to microwave radiation at a 450 W power level for 10 seconds before performing a TPR experiment. This was done to observe if microwave pre-treatment induces any changes to the reducibility of the catalysts. The TPR profiles were recorded and they are shown in Figure 4.9. Table 4.4 lists the exact temperatures at which reduction occurs for the different samples.

It can be seen from Figures 4.9 and 4.10 and Table 4.4 that even after microwave pre-treatment in the solid-state, the reducibility of the catalysts follows the same pattern. To examine any changes in the positions at which these peaks occur, a plot (Figure 4.10) of the loading of potassium versus the maximum temperature at which Peak 1 occurs was done for both microwave pre-treated and non-pre-treated samples. From this plot and Table 4.4, it is noted that the reduction of Fe_2O_3 to Fe_3O_4 increased almost linearly with potassium loading both with and without microwave exposure. This shows that microwave pre-treatment does not affect the reducibility of these catalysts.

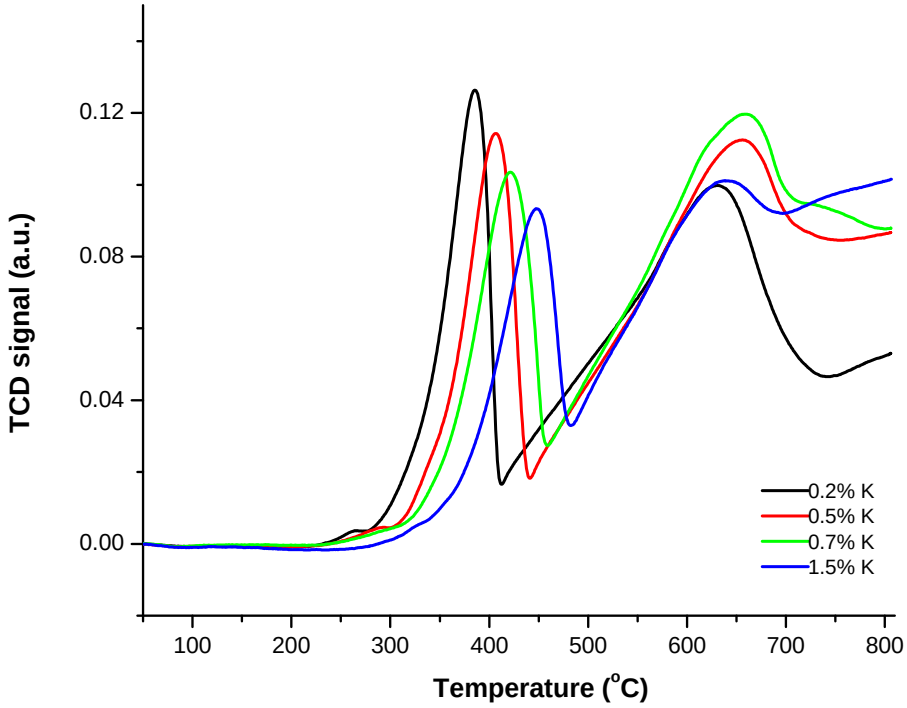

Figure 4.9 TPR profiles of 0.2 K/Fe-MW, 0.5 K/Fe-MW, 0.7 K/Fe-MW and 1.5 K/Fe-MW catalysts after microwave pre-treatment. Microwave pre-treatment conditions: 450 W, 10 seconds.

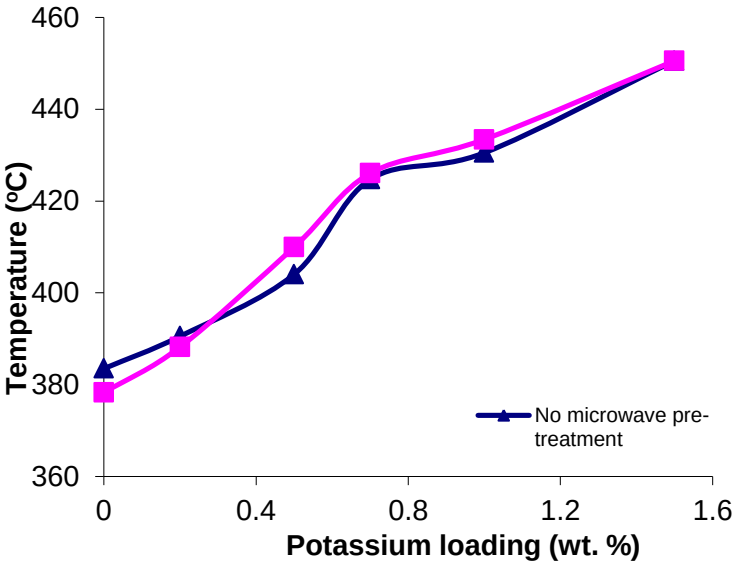

Figure 4.10 Increases in the first reduction temperature ($Fe^{3+} \rightarrow Fe^{2+}$) with an increase in the loading of potassium, as seen in TPR.

4.3.5 Temperature programmed surface reaction-mass spectrometry (TPSR-MS)

4.3.5.1 Blank run

FTS is a typical CO hydrogenation reaction carried out over a heterogeneous catalyst, which starts from the dissociation of CO and H_2 on transient metal surfaces and follows with the hydrogenation and polymerization of surface carbon species.[21] Using temperature-programmed techniques, mechanistic information can be inferred for the FTS reaction. A temperature programmed surface reaction (TPSR) is one technique that is useful in this regard. It has the advantage of being surface sensitive and therefore useful when determining the number and types of active sites present on the surface of a catalyst.

Figure 4.11 shows typical profiles of the effluent mole fractions for the components CH_4, H_2O, CO_2 and CO as obtained from a quadrupole mass spectrometer (QMS) during a TPSR experiment. For water analysis, mass-to-charge ratios (m/z) of 17 and 18 were monitored as shown. In the TPSR experiment, CO was adsorbed for an hour on a pre-reduced 1.5K/Fe catalyst. The adsorbed CO was then hydrogenated as a function of temperature and the evolved species were monitored using a QMS and a gas chromatograph fitted with an FID. It is known that CO adsorption can occur either molecularly (eqn 4.3) or dissociatively (eqn 4.4), while the desorption of CO occurs directly out of the molecularly adsorbed state (eqn 4.5) or after the recombination of adsorbed atomic carbon and oxygen (eqn 4.6). The recombination of adsorbed carbon and oxygen leads to the formation of CO as well as CO_2 (eqn 4.6 and 4.7).[22] CO_2 formation can also occur *via* the oxidation of CO (eqn 4.8)

$$CO_{(g)} + * \rightarrow CO_{ads} \quad (4.3)$$

$$CO_{(g)} + 2* \rightarrow C_{ads} + O_{ads} \quad (4.4)$$

$$CO_{ads} \rightarrow CO_{(g)} + * \quad (4.5)$$

$$C_{ads} + O_{ads} \rightarrow CO_{ads} + * \rightarrow CO_{(g)} + 2* \quad (4.6)$$

$$C_{ads} + 2O_{ads} \rightarrow CO_{ads} + O_{ads} + * \rightarrow CO_{2,ads} + 2* \rightarrow CO_{2\,(g)} + 3* \quad (4.7)$$

$$CO_{ads} + O_{ads} \rightarrow CO_{2(g)} \quad (4.8)$$

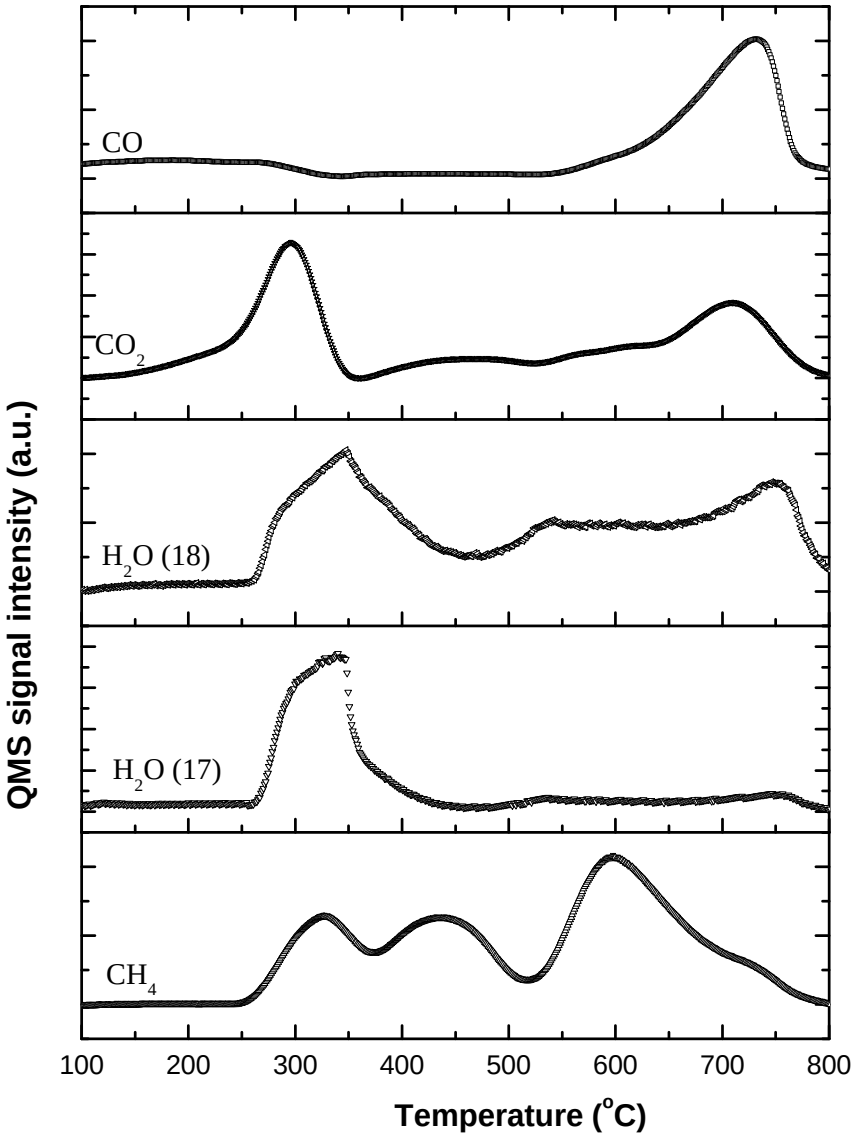

Figure 4.11 Effluent mole fractions of the components CH_4, H_2O (m/z = 17), H_2O (m/z = 18), CO_2 and CO formed during the TPSR experiment using the 1.5 K/Fe catalyst.

From the profiles shown in Figure 4.11 it can be appreciated that CH_4 formation starts at 251 ^oC and stops at 763 ^oC when the 1.5 K/Fe catalyst is being used. Within this temperature range, the simultaneous evolution of H_2O, CO_2 and CO is noted as the adsorbed CO is hydrogenated. According to our experiments, which were performed in order to investigate the adsorption characteristics of CO on iron, most of the CO was adsorbed dissociatively as

shown by equation 4.4 while only a small fraction was adsorbed in the molecular state according to equation 4.3. The CO profile shown in Figure 4.11 reveals the presence of two signals, a small but broad peak at 180 ^{o}C and a large peak with a maximum at 731 ^{o}C. The CO signal at 180 ^{o}C is due to the desorption of molecularly adsorbed CO, while the signal observed at 731 ^{o}C is due to CO desorption after recombination of dissociatively adsorbed CO fragments leading to CO and CO_2 formation (eqn 4.6 and 4.7). This is confirmed by an analysis of the CO_2 profile which is displayed in the same figure. Recombination of dissociatively adsorbed CO on Fe(100) is known to occur in the temperature range from 427 ^{o}C to 627 ^{o}C.[23-25] The CO_2 signal at 280 ^{o}C is due oxidation of CO (eqn 4.8) with H_2O or formed via the water gas shift (WGS) reaction.

The methane evolution rate (due to reaction of carbon with H_2) as recorded using both an FID detector and a quadrupole mass spectrometer (QMS) during the TPSR experiment is displayed in Figure 4.12a and 4.12b, correspondingly. The recorded signals are broad, indicating that several overlapping peaks coexist. Differences in the signals recorded using the FID and the QMS are mainly due to the overlapping of peaks. To quantitatively analyse the overlapping peaks, the TPSR profiles were fitted with Gaussian curves to yield several peaks. From the deconvoluted spectra, five CH_4 peaks are observed, signifying that there were five types of carbon species deposited on the catalyst surface before it was hydrogenated to form methane. These five kinds of carbon species are assigned to α_1, α_2, β, γ and δ (Table 4.5) and the information obtained from these peaks is discussed in subsequent sections. Eliason and Bartholomew[26] also used a similar method when performing a quantitative analysis of their overlapping peaks for unpromoted and K-promoted Fe FT catalysts from TPSR. The mass spectrometry experiment (see Figure 4.12b) was performed simultaneously to verify the identity of the species evolved in the TPSR experiment. Most of the experiments in this work were then performed using a flame ionization detector (FID) since it was observed that the results recorded using the FID were comparable to those obtained using a quadrupole mass spectrometer (see Figure 4.12). Therefore, the use of the QMS in this work has been qualitative and not quantitative.

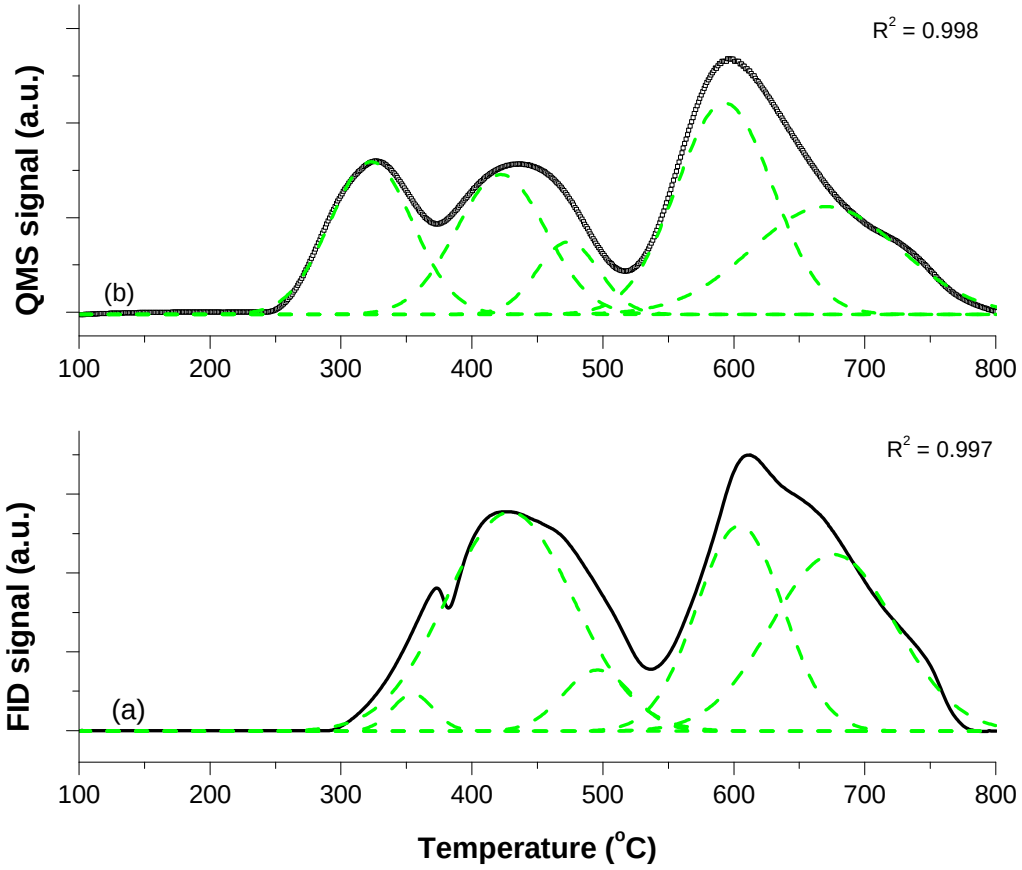

Figure 4.12 Methane profiles recorded during the TPSR experiment using (a) an FID detector and (b) a QMS spectrometer for the 1.5 K/Fe catalyst before MW pre-treatment.

4.3.5.2 The effect of potassium (no microwave pre-treatment)

TPSR profiles for methane evolution from the catalysts with varying loadings of potassium are compared in Figure 4.13. It can be seen from this figure that CH_4 peaks from the 0K/Fe catalyst lie in the temperature range of 300–700 ^{o}C, while the peaks from the 1.5K/Fe catalyst lie in the temperature range of 300–785 ^{o}C. It is evident that the CH_4 peaks shift to higher temperatures as the loading of potassium is increased. The peaks are quite broad, indicating that several overlapping peaks coexist. Just like in the preceding section, these overlapping peaks were analysed by fitting Gaussian curves that yielded several peaks and the corresponding peak parameters are listed in Table 4.5.

The five CH_4 signals observed from the deconvoluted spectra signify that there were five kinds of carbon species deposited on the catalyst surface before hydrogenation to form methane. The five peaks are assigned as the α_1, α_2, β, γ, and δ species, corresponding to: two forms of adsorbed atomic carbon, amorphous surface methylene chains or films, bulk iron carbide, or graphitic carbon. Peak temperatures increase in that same order, i.e., in the order of decreasing reactivity with H_2. The peak assignments of these species are based on previous literature reports.[27] This assessment was done to establish if a correlation exists between the active surface carbon species formed on the catalyst and the amount of potassium loaded in the catalyst. The adsorption of CO on iron single crystals has been reported in the literature by quite a few researchers.[23-25,28] Nassir *et al.*[23], Moon *et al.*[24,28] as well as Benziger and Madix[25] carried out temperature programmed desorption (TPD) experiments with CO on a Fe(100) surface and they reported four desorption peaks. The three peaks at low temperatures were identified to be due to the desorption of CO from the molecularly adsorbed state, whereas the high temperature peak was due to a recombination of dissociatively adsorbed CO fragments.[24]

From the data in Figure 4.13 and Table 4.5 it is evident that the overall amount of CH_4 evolved increases with the content of the potassium promoter in the catalyst. This observation is rather unusual since certain catalytically active sites are expected to be blocked as the loading of potassium increases, as reported elsewhere.[22] However, the figure shown and the respective peak areas indicate that this increase in CH_4 is largely due to the γ- and δ-species which are favoured at high potassium loadings. The highest percentage of methane formed from α carbon is seen when K = 0.2 wt. %, and thereafter the percentage of CH_4 decreases steadily with an increase in potassium content. In contrast, the amount of methane formed from both carbide carbon and graphitic carbon increases as the loading of potassium is increased.

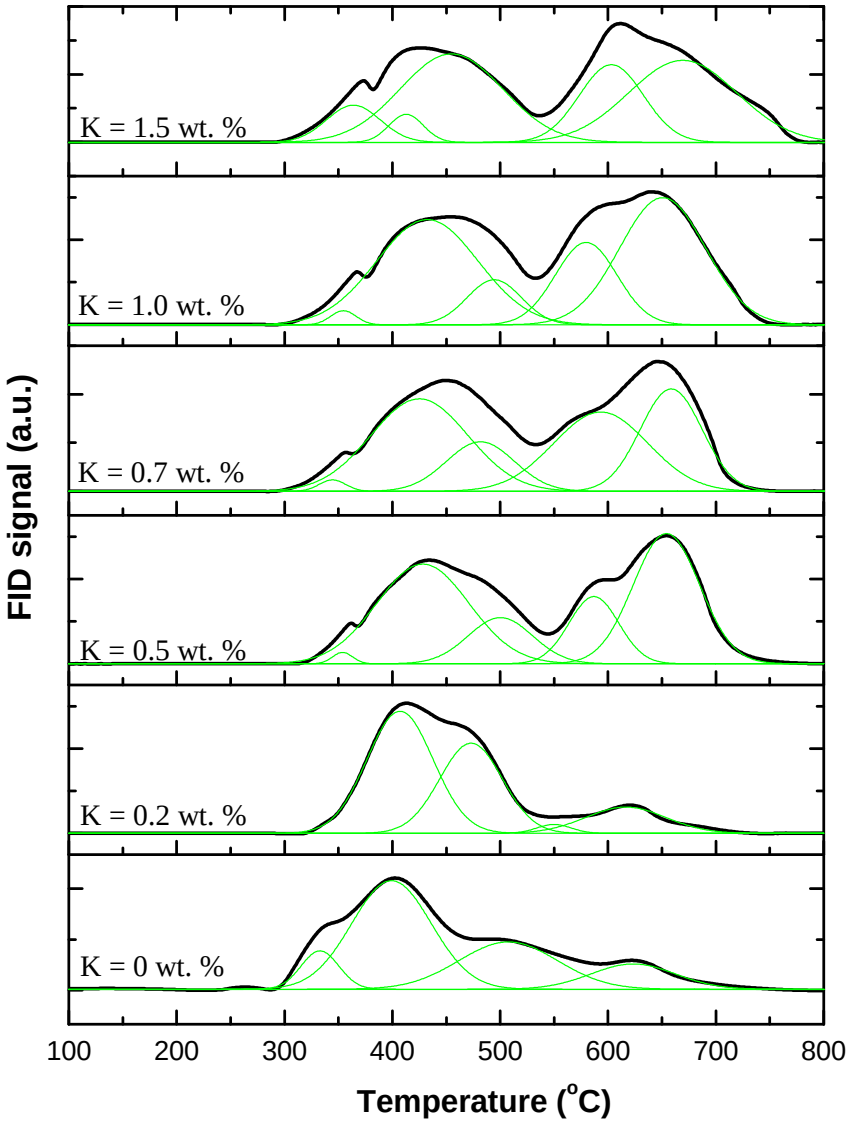

Figure 4.13 TPSR profiles for CH_4 evolution for 0K/Fe, 0.2K/Fe, 0.5K/Fe, 0.7K/Fe, 1.0K/Fe and 1.5K/Fe catalysts. These profiles were recorded before MW treatment. The fitted Gaussian curves are shown as green dotted lines.

Table 4.5 Relative percentage compositions of methane produced from the various carbon species when different weight percentages of potassium are loaded in the catalysts. These values were obtained in the non-microwaved samples.

Catalyst composition (wt. %)	Peak parameters[a,b]					Total CH_4 evolved[c] ($\mu mol\ g^{-1}$)
	carbidic α_1	carbidic α_2	amorphous β	carbide γ	graphitic δ	
0K/Fe	-	8.6/333	50.9/399	27.8/507	12.7/623	32
0.2K/Fe	-	50.9/407	34.9/473	1.9/550	13.2/616	35
0.5K/Fe	0.9/354	37.7/428	12.2/500	13.7/587	35.5/654	52
0.7K/Fe	1.7/344	33.9/425	12.7/482	28.3/593	23.4/658	50
1.0K/Fe	1.3/355	36.2/432	8.3/494	17.2/580	37.0/651	62
1.5K/Fe	7.0/359	18.4/416	20.3/477	23.6/604	30.7/675	68

[a] The TPSR profiles were fitted with multiple Gaussian shapes.

[b] The relative percentage composition (%) / the peak position (^oC) of individual carbon species.

[c] The total CH_4 evolved was obtained by integrating the entire CH_4 evolution curve and then using methane calibration.

4.3.5.3 The microwave pre-treatment effect

The effect of microwave pre-treatment on the precipitated catalyst's surface properties was investigated using TPSR. Figure 4.14 summarizes methane evolution profiles for the various catalysts that were microwaved for 10 seconds (450 W power level) prior to performing TPSR experiments. Table 4.6 lists the observed peak temperatures and the relative percentage contributions from the various carbon species obtained from the deconvoluted microwaved and non-microwaved samples. In Figure 4.14 it was observed that MW pre-treatment reveals the presence of all five carbon species in the 0.2K/Fe-MW catalyst. This is not seen in the non-microwaved sample (see Figure 4.13).

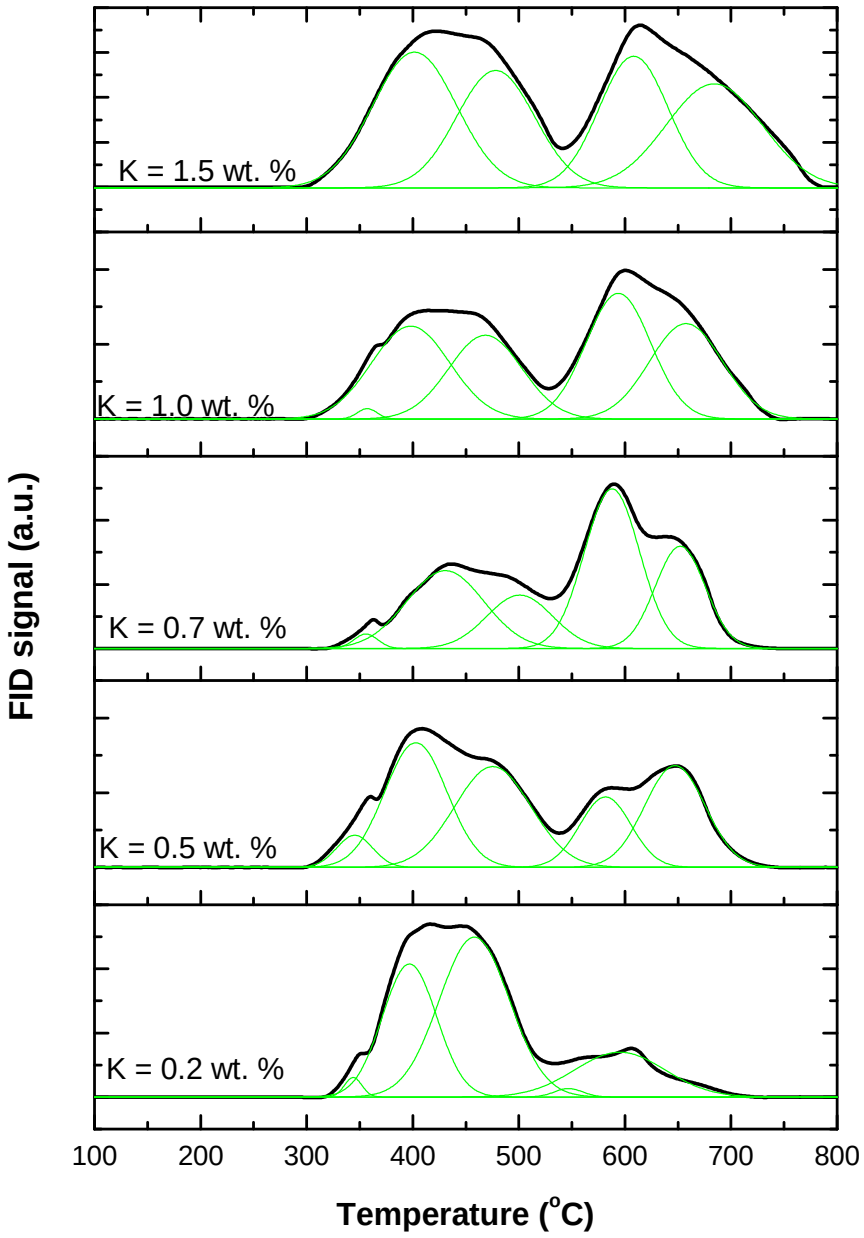

Figure 4.14 TPSR profiles for CH_4 evolution for 0K/Fe-MW, 0.2K/Fe-MW, 0.5K/Fe-MW, 0.7K/Fe-MW, 1.0K/Fe-MW and 1.5K/Fe-MW catalysts. Microwave pre-treatment conditions: 450 W power level, 10 seconds. The fitted Gaussian curves are shown as green lines.

Table 4.6 A comparison of the relative percentage composition before and after microwave pre-treatment. Microwave pre-treatment conditions: 450 W power level, 10 seconds.

Catalyst	Peak parameters[a,b]					Total CH_4 evolved[c] ($\mu mol\ g^{-1}$)
	carbidic α_1	carbidic α_2	amorphous β	carbide γ	graphitic δ	
0.2K/Fe	-	50.9/407	34.9/473	1.9/550	13.2/616	35
0.2K/Fe-MW	1.6/343	44.4/405	34.3/467	1.7/542	18.0/593	37
0.5K/Fe	0.9/354	37.7/428	12.2/500	13.7/587	35.5/654	52
0.5K/Fe-MW	4.4/345	29.5/403	29.1/475	13.6/582	23.4/647	65
0.7K/Fe	1.7/344	33.9/425	12.7/482	28.3/593	23.4/658	50
0.7K/Fe-MW	1.4/356	25.2/431	14.8/501	37.1/588	21.5/652	68
1.0K/Fe	1.3/355	36.2/432	8.3/494	17.2/580	37.0/651	62
1.0K/Fe-MW	1.8/358	24.0/399	21.4/469	28.9/594	23.9/658	71
1.5K/Fe	7.0/359	18.4/416	20.3/477	23.6/604	30.7/675	68
1.5K/Fe-MW	-	28.2/401	23.7/477	23.3/608	24.8/684	77

[a] The TPSR profiles were fitted with multiple Gaussian shapes.

[b] The relative percentage composition (%) / the peak position (^oC) of individual carbon species.

[c] The total CH_4 evolved was obtained by integrating the entire CH_4 evolution curves and then using methane calibration.

Considering the catalysts with potassium loading of 0.2 and 0.5 wt. %, the overall CH_4 evolved increases for the catalysts that were modified using microwave pre-treatment relative to their un-modified counterparts. It was observed that 37 µmol g^{-1} CH_4 were produced overall from the 0.2K/Fe-MW catalyst, and 35 µmol g^{-1} CH_4 were recorded from the 0.2K/Fe catalyst. Only a marginal difference in values is noted. At 0.5 wt. % potassium loading a remarkable CH_4 signal equivalent to 65 µmol g^{-1} was recorded for the microwave pre-treated catalyst, while only 52 µmol g^{-1} CH_4 were obtained from the un-modified catalyst. This is equivalent to a 25% increase in the hydrocarbon content which is attributed to the MW pre-treatment effect. Comparing the contributions from the different carbon species for the 0.5K/10Fe/SiO_2 sample shows that MW modification increases the CH_4 content produced from β-carbon species. The formation of adsorbed atomic carbon (C_α) and graphitic carbon (C_δ) is suppressed in the microwaved sample, while iron carbides formation is unaffected (see Figure 4.15).

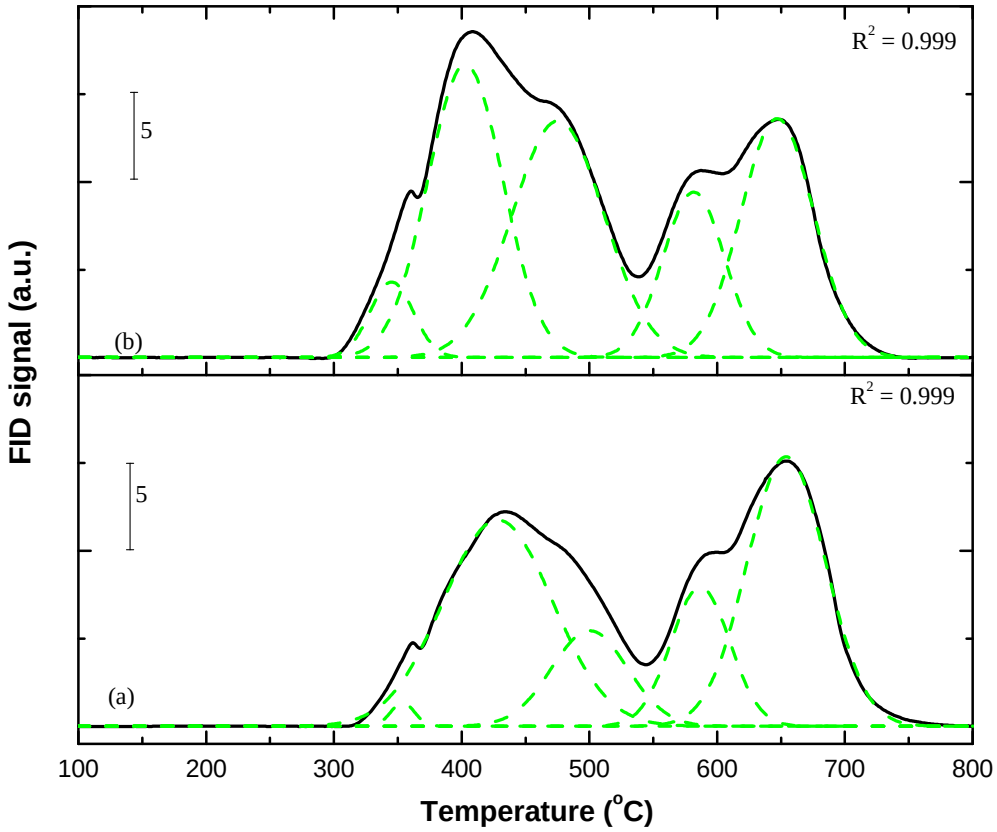

Figure 4.15 TPSR profiles of (a) 0.5K/Fe and (b) 0.5K/Fe-MW showing the individual peak contributions from the various carbon species.

Increases in CH_4 production due to modification of the catalysts in the solid-state were also seen at potassium loadings of 0.7 and 1.0 wt. %. An increase of 35% was seen for the former while a 14% rise was recorded at the latter K loading. These increases were computed from CH_4 signals corresponding to 68 and 50 µmol g^{-1} evolved from 0.7K/Fe-MW and 0.7K/Fe catalysts and 71 and 62 µmol g^{-1} CH_4 for 1.0K/Fe-MW and 1.0K/Fe catalysts. Figure 4.16 and Figure 4.17 shows that at these potassium loadings MW pre-treatment favours CH_4 formation from surface methylene chains and bulk iron carbides. CH_4 formation from α- and δ-carbon species declines in the modified samples. The CH_4 peak produced from the MW favoured γ-carbon species appears at 652 ^oC and 656 ^oC for the 0.7K/Fe-MW and the 1.0K/Fe-MW catalysts, correspondingly. MW pre-treatment of the 1.5K/Fe catalyst inhibits the formation of the α_1-carbon species (see Figure 4.18). This could be due to the presence of excess potassium ions on the surface of the catalyst.

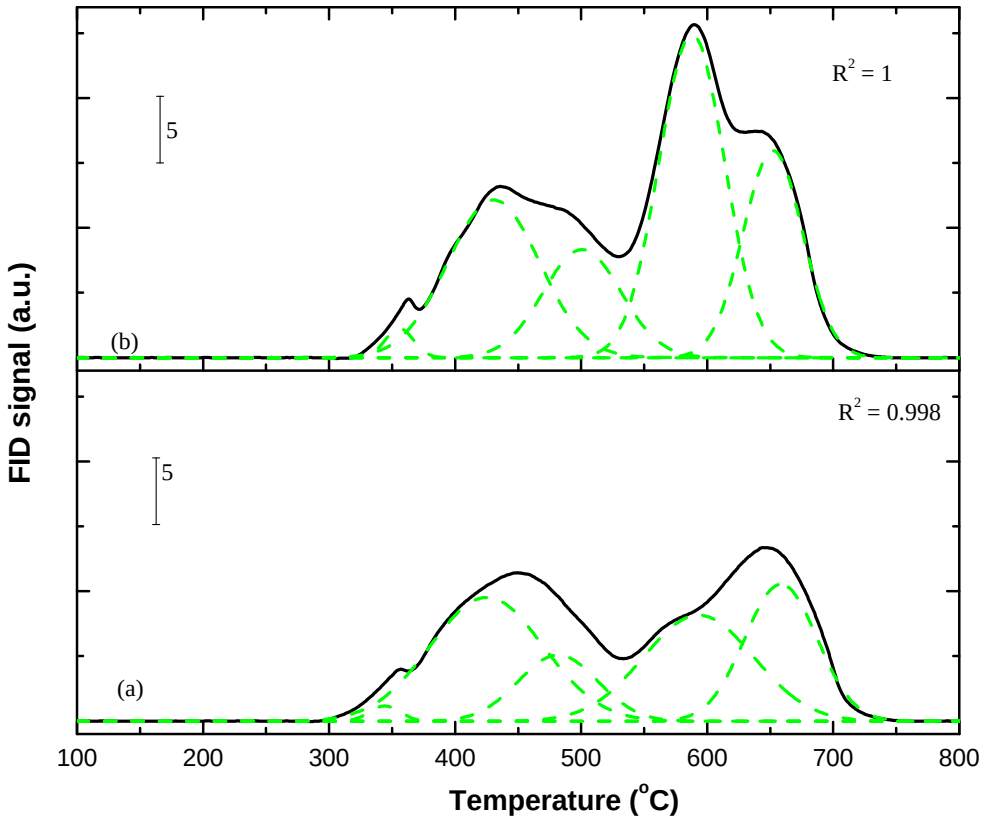

Figure 4.16 TPSR profiles of (a) 0.7K/Fe and (b) 0.7K/Fe-MW showing the individual peak contributions from the various carbon species.

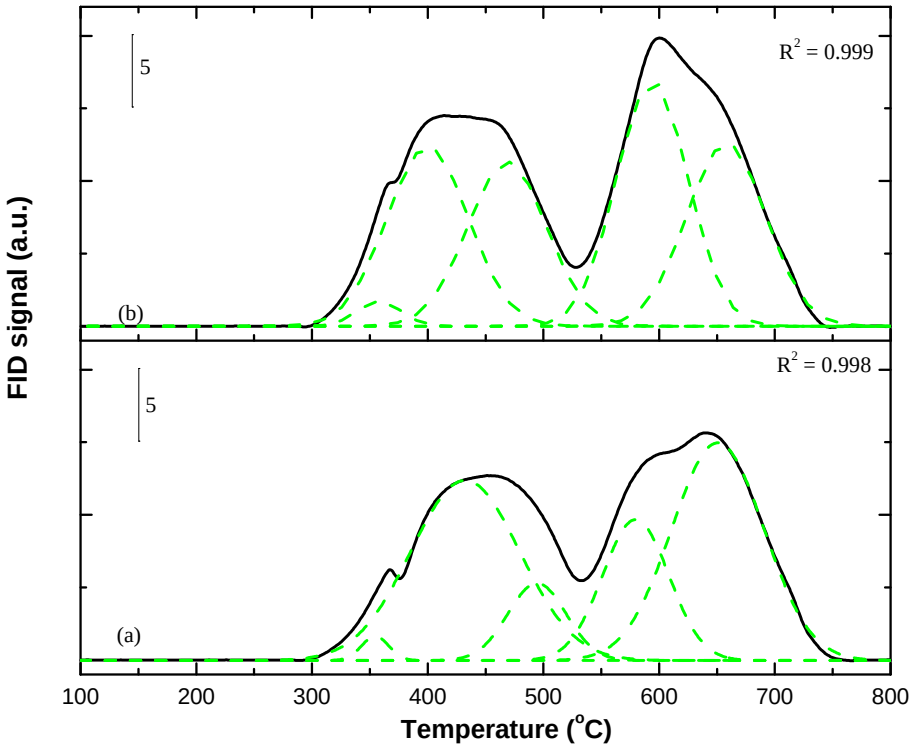

Figure 4.17 TPSR profiles of (a) 1.0K/Fe and (b) 1.0K/Fe-MW showing the individual peak contributions from the various carbon species.

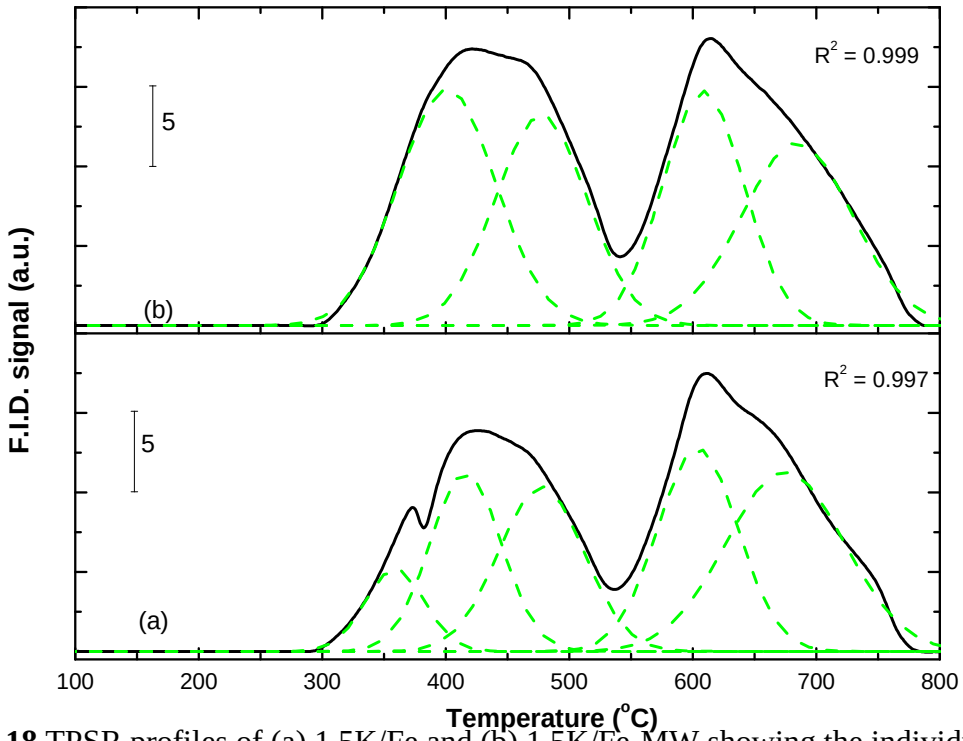

Figure 4.18 TPSR profiles of (a) 1.5K/Fe and (b) 1.5K/Fe-MW showing the individual peak contributions from the various carbon species.

Figure 4.19 summarizes the percentage increases in the total CH_4 evolved that were induced purely by microwave pre-treatment of the different catalysts. This graph was achieved by expressing the difference in the total CH_4 produced before and after microwave pre-treatment as a percentage and then plotting the data as a function of the loading of potassium. As shown in the figure, MW pre-treatment increases the total CH_4 evolved at all loadings of potassium. A 6% increase at 0.2 wt. % of potassium is followed by a 25% increase at 0.5 wt. % loading of potassium. The highest percentage increase was found at a loading of 0.7 wt. % potassium – a change of 35%. Higher loadings of 1.0 and 1.5 wt. % K produced less methane, but still gave increases of 14%. It is clear that the MW pre-treatment effect is dependant on the loading of potassium in precipitated catalysts, with 0.7 wt. % K proving to be the optimum loading for the experiments performed in this work.

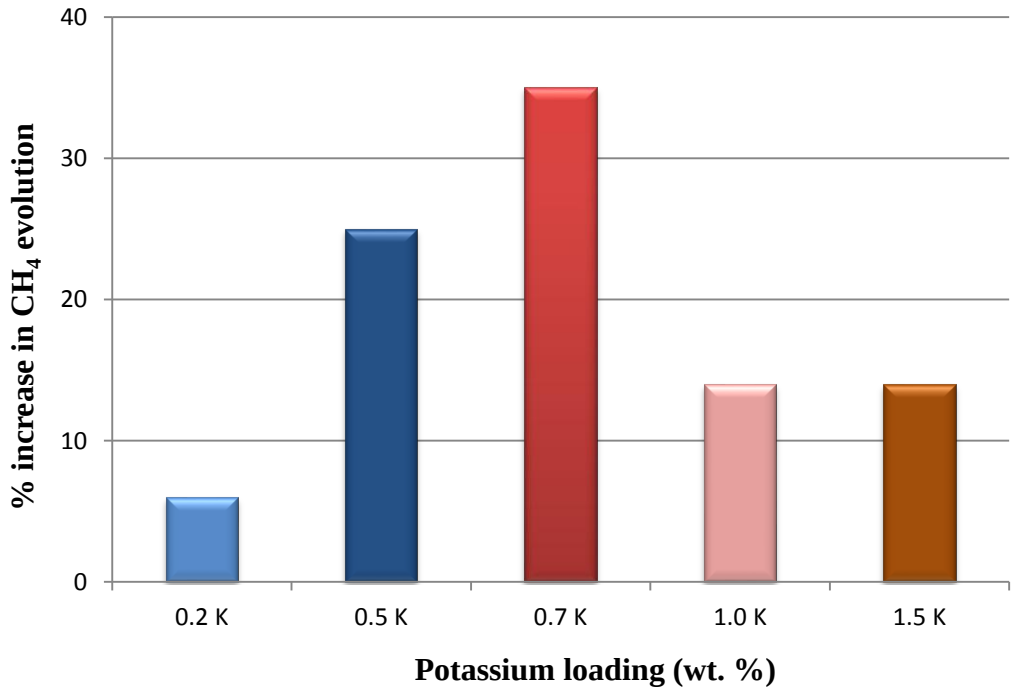

Figure 4.19 Percentage increases in methane evolution induced by microwave pre-treatment for the various loadings of potassium.

4.3.5.4 The effect of the MW irradiation time

To gain further insight into the microwave pre-treatment effect, the microwave irradiation time was increased to 40 seconds. Reduction profiles for the catalysts were recorded and they are shown in Figure 4.20. Tabulated in Table 4.7 are the temperatures maxima for the corresponding reduction steps. Peak 1 shows a marginal shift to high temperatures as the microwave exposure time is increased. Peak 2 remains relatively unaffected by microwave pre-treatment.

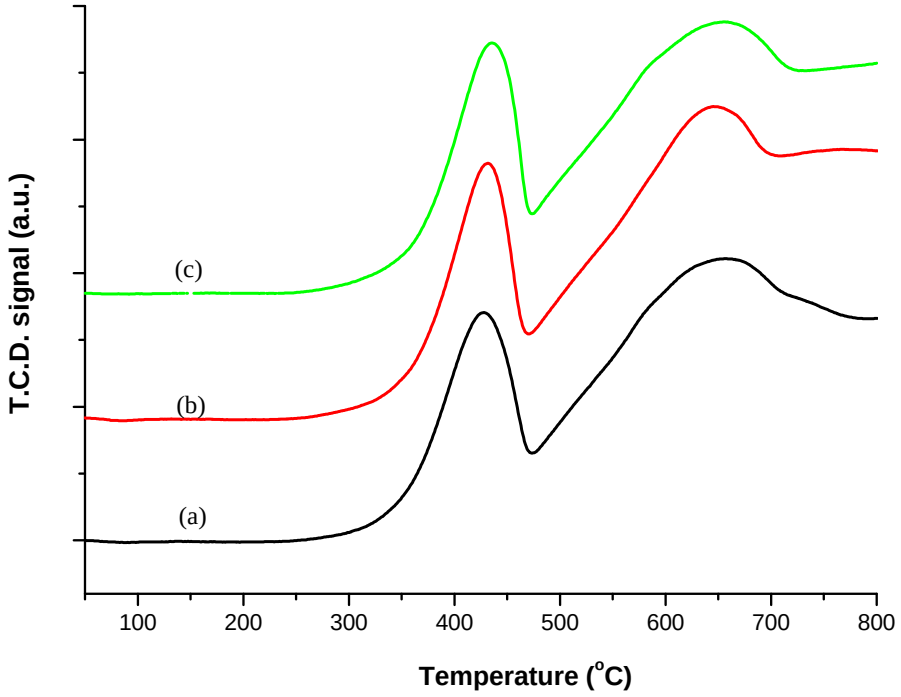

Figure 4.20 Reduction profiles for the 0.7K/Fe catalyst that was microwaved for (a) 0 seconds, (b) 10 seconds and (c) 40 seconds.

Table 4.7 Reduction temperatures for the H_2 TPR profiles shown in Figure 4.20.

MW irradiation time	TPR peak maximum (°C)	
	Peak 1	Peak 2
0 seconds	426	658
10 seconds	431	654
40 seconds	436	656

The effect of the pre-treatment time has also been studied using TPSR to see if it affected the total CH_4 content evolved. The microwave irradiation time was increased from 10 seconds to 20 seconds, 40 seconds, 2 minutes, 5 minutes and 10 minutes (see Figure 4.21 and Appendix C). The microwave power level was maintained at 450 W. This study was conducted using the 0.7K/Fe catalyst as it showed the highest microwave pre-treatment effect in the earlier studies (section 4.3.5.2). MW pre-treatment caused an initial 35% increase in the total CH_4 evolved (after 10 seconds), but increasing the microwave exposure time up to 600 seconds (10 minutes) generally did not improve the methanation rate. This data suggests that the unsupported K/Fe catalysts studied in this work are not influenced by the irradiation time; the microwave effect is observed immediately.

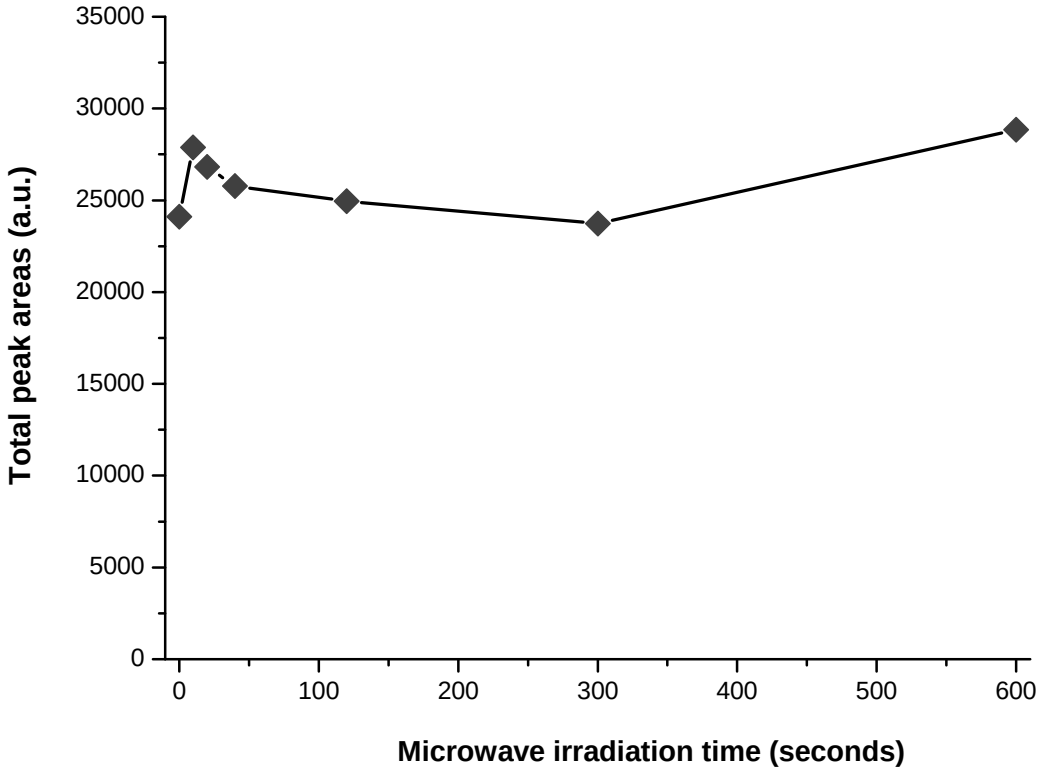

Figure 4.21 Total peak areas corresponding to methane evolved from the 0.7K/Fe-FW catalyst. The catalyst was irradiated for 0 seconds, 10 seconds, 20 seconds, 40 seconds, 2 minutes, 5 minutes and 10 minutes.

4.4 Conclusions

The effects of potassium on microwave-modified precipitated catalysts were investigated by analysing the bulk and surface properties of the catalysts before and after microwave pre-treatment. Bulk properties that were studied include the morphology, texture, structure and reducibility of the catalyst, while surface studies focused on adsorption. A range of potassium weight loadings on precipitated Fe catalysts were investigated (0–1.5 wt. % K).

Without any microwave pre-treatment, potassium was seen to give an increase in the iron crystallite size. This increase in particle size is believed to be partly responsible for inhibiting the reducibility of iron seen in TPR. After pre-treatment the catalysts still displayed similar bulk properties as did their un-modified counterparts. This shows that microwave pre-treatment did not modify the bulk properties of these catalysts in way.

Microwave pre-treated catalysts displayed different CO adsorption characteristics when compared to the un-modified catalysts with similar compositions. Larger hydrocarbon quantities were evolved in the TPSR from all the microwave modified catalysts when compared to their non-microwaved counterparts. The increase in hydrocarbon content rose from 6% for the 0.2 wt. % K catalyst and continued to rise with the loading of potassium. The content eventually dropped to 14% for the 1.0 and 1.5 wt. % K catalysts. The 0.7 wt. % K catalyst was shown to have the optimum loading after microwave heating as displayed by an increase of 35% in the total CH_4 content.

In all the studied samples, MW pre-treatment was seen to promote the formation of surface methylene chain and bulk iron carbides. These studies were done in the TPSR. The formation of graphitic-like carbon and adsorbed atomic carbon either remained unchanged or decreased in the microwave modified samples.

4.5 References

(1) Xiong, H.; Zhang, Y.; Wang, S.; Li, J. *Catal. Commun.* **2005**, *6*, 512.

(2) Ge, Q.; Neurock, M.; Wright, H. A.; Srinivasan, N. *J. Phys. Chem. B.* **2002**, *106*, 2826.

(3) Luo, M.; Davis, B. H. *Appl. Catal. A: Gen.* **2003**, *246*, 171.

(4) Davis, B. H. *Catal. Today* **2003**, *84*, 83.

(5) Tobias, H. J.; Beving, D. E.; Ziemann, P. J.; Sakurai, H.; Zuk, M.; McMurry, P. H.; Zarling, D.; Waytulonis, R.; Kittelson, D. B. *Environ. Sci. Technol.* **2001**, *35*, 2233.

(6) Ngantsoue-Hoc, W.; Zhang, Y.; O'Brien, R. J.; Luo, M.; Davis, B. H. *Appl. Catal. A: Gen.* **2002**, *236*, 77.

(7) Li, S.; Krishnamoorthy, S.; Li, A.; Meitzner, G. D.; Iglesia, E. *J. Catal.* **2002**, *206*, 202.

(8) Motjope, T. R.; Dlamini, H. T.; Hearne, G. R.; Coville, N. J. *Catal. Today* **2002**, *71*, 335.

(9) Bukur, D. B.; Lang, X.; Mukesh, D.; Zimmerman, W. H.; Rosynek, M. P.; Li, C. *Ind. Eng. Chem. Res.* **1990**, *29*, 1588.

(10) Yang, Y.; Xiang, H.; Xu, Y.; Bai, L.; Li, Y. *Appl. Catal. A: Gen.* **2004**, *266*, 181.

(11) Jacobs, G.; Chaney, J. A.; Patterson, P. M.; Das, T. K.; Maillot, J. C.; Davis, B. H. *J. Synchrotron Radiat.* **2004**, *11*, 414.

(12) Linganiso, L. Z. PhD. Thesis, University of the Witwatersrand, 2008.

(13) Recommendations, I. *Pure Appl. Chem.* **1985**, *57*, 603.

(14) Recommendations, I. *Pure Appl. Chem.* **1994**, *66*, 1739.

(15) Sing, K. S. W.; Everett, D. H.; Haul, R. A. W.; Moscou, L.; Pierotti, R. A.; Rouquerol, J.; Siemieniewska, T. *Pure Appl. Chem.* **1985**, *57*, 603.

(16) Barrett, E. P.; Joyner, L. G.; Halenda, P. P. *J. Am. Chem. Soc.* **1951**, *73*, 373.

(17) Luo, M.; Hamdeh, H.; Davis, B. H. *Catal. Today* **2009**, *140*, 127.

(18) Rankin, J. L.; Bartholomew, C. H. *J. Catal.* **1986**, *100*, 533.

(19) Lund, C. R. F.; Dumesic, J. A. *J. Phys. Chem.* **1982**, *87*, 130.

(20) Li, C. Ph.D. Dissertation, Texas A & M University, 1988.

(21) Zhang, C.; Zhao, G.; Liu, K.; Yang, Y.; Xiang, H.; Li, Y. *J. Mol. Catal. A: Chem.* **2010**, *328*, 35.

(22) Graf, B.; Muhler, M. *Phys. Chem. Chem. Phys.* **2011**, *13*, 3701.

(23) Nassir, M. H.; Fruhberger, B.; Dwyer, D. J. *Surf. Sci.* **1994**, *312*, 115.

(24) Moon, D. W.; Dwyer, D. J.; Bernasek, S. L. *Surf. Sci.* **1985**, *163*, 215.

(25) Benziger, J.; Madix, R. J. *Surf. Sci.* **1980**, *94*, 119.

(26) Eliason, S. A.; Bartholomew, C. H. In *Studies in surface science and catalysis*; Bartholomew, C. H., Fuentes, G. A., Eds.; Elsevier: Amsterdam, 1997; Vol. 111, p 517.

(27) Xu, J.; Bartholomew, C. H. *J. Phys. Chem. B.* **2005**, *109*, 2392.

(28) Moon, D. W.; Bernasek, S. L.; Dwyer, D. J.; Gland, J. L. *J. Am. Chem. Soc.* **1985**, *107*, 4363.